

How Bumps on Whale Flippers Delay Stall: An Aerodynamic Model

Ernst A. van Nierop, Silas Alben, and Michael P. Brenner

School of Engineering and Applied Sciences, Harvard University, Cambridge, Massachusetts 02138, USA

(Received 20 June 2007; published 7 February 2008)

Wind tunnel experiments have shown that bumps on the leading edge of model humpback whale flippers cause them to “stall” (i.e., lose lift dramatically) more gradually and at a higher angle of attack. Here we develop an aerodynamic model which explains the observed increase in stall angle. The model predicts that as the amplitude of the bumps is increased, the lift curve flattens out, leading to potentially desirable control properties. We find that stall delay is insensitive to the wavelength of the bumps, in accordance with experimental observations.

DOI: [10.1103/PhysRevLett.100.054502](https://doi.org/10.1103/PhysRevLett.100.054502)

PACS numbers: 47.85.Gj, 47.50.Cd, 47.63.M–

Humpback whales [*Megaptera novaeangliae*, see Fig. 1(a)] are particularly agile whales, capable of performing rolls and loops under water [1,2]. Their agility has been attributed to the bumpy tubercles on the leading edge of their pectoral flippers [2]. Inspired by this uncommon leading-edge design, Miklosovic *et al.* tested model flippers in wind tunnels, and found that the bumps lead to an increase in stall angle of up to 40% without compromising lift or drag [3]. Later experiments showed that bumps make the onset of stall much more gradual [4,5]. Model aircraft builders have already adjusted wing designs to take advantage of these desirable control properties [6], but the mechanism remains unclear. In this Letter we demonstrate that a model based on standard aerodynamic theory explains most of the experimentally observed phenomena.

Leading-edge bumps on flippers or wings have been compared to vortex generators [3], which are small objects placed on a wing that inject momentum into the boundary layer (i.e., making it turbulent) to delay flow separation [7]. However, it is implausible that bumps on the flippers act as vortex generators since both the wavelength and amplitude of the bumps are much larger than the boundary layer thickness. Here we propose a different mechanism: we demonstrate that the bumps alter the pressure distribution on the wing such that separation of the boundary layer is delayed behind bumps. This ultimately leads to a *gradual* onset of stall and a larger stall angle.

To understand the role of the bumpy tubercles, we consider a simple model of a smooth wing, and then show how the aerodynamic properties of the wing are modified when bumps are added. Our model considers a wing whose chord varies on a length scale large compared with its thickness. Working in this limit allows us to analytically capture the unseparated flow around the wing up to the attack angles where separation occurs. We employ an empirical separation criterion derived for flow around flat plates, which is approximately correct in the thin plate limit. Since in this long-wavelength limit there is no spanwise flow, flow separation at each wing section is assumed to depend on the upstream flow conditions rather than the flow over neighboring sections. For the smooth wing we use a clas-

sical elliptic wing [8]; each cross section of the wing is described by a Joukowski profile; see Fig. 1(c), [9]. For a typical humpback whale lunging speed of $U_0 = 2.6$ m/s and ocean viscosity of $\nu = 1.35 \times 10^{-6}$ m²/s, the flow around the wing has typical Reynolds number $Re > 5 \times 10^5$ [3], and is composed of two different regimes. Near the wing, there is a (turbulent) boundary layer while outside of the boundary layer the flow is well-approximated by potential flow, where the circulation Γ is determined by the Kutta condition [9]

$$\Gamma = -\pi U_0 \left(c + \frac{4}{3\sqrt{3}} t \right) \alpha^e + O((\alpha^e)^3, t^3) \quad (1)$$

Here U_0 is the uniform flow velocity, c is the chord length, t is the thickness, and α^e is the effective angle of attack [see Fig. 1(c)]. Both the chord length and the wing thickness taper off from the root of the wing to the tip [$y = 0$ and $y = s$ or $\theta = \pi/2$ and $\theta = 0$ respectively, see Fig. 1(b)] such that their ratio t/c is constant. For an elliptic wing, $c(\theta) = c_0 \sin\theta$ and $t(\theta) = t_0 \sin\theta$.

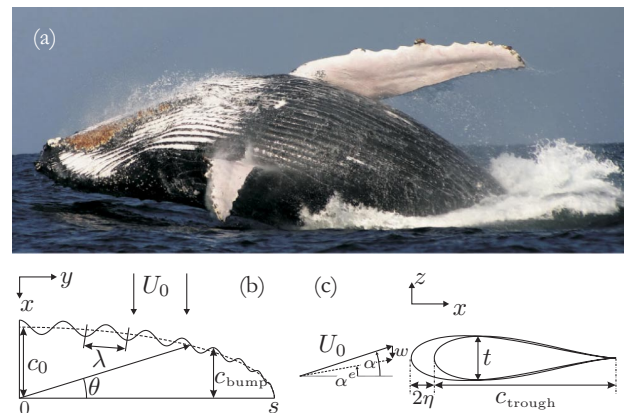


FIG. 1 (color online). (a) Humpback whale lunging for food; note the bumps on the leading edge of the pectoral fins. Photograph by Brett Atkins, obtained from www.dreamstime.com. Sketch of the flipper geometry: (b) the planform from above; (c) cross section of a bump and trough of amplitude η .

Equation (1) implies that the variation of the chord and thickness along the wing causes a variation in the circulation Γ . Such spanwise changes in Γ generate a sheet of streamwise vortices behind the wing, which causes a downwash w —an oncoming downward flow—at each wing cross section [see Fig. 1(c)]. This downwash causes the effective angle of attack to vary along the wing,

$$\alpha^e = \alpha - \frac{w}{U_0}. \quad (2)$$

The magnitude of the downwash can be calculated using lifting-line theory, which allows us to represent the wing as a single vortex line of varying strength along the span [8]

$$w = \frac{1}{4\pi} \int_{-s}^s \frac{d\Gamma/dy'}{y - y'} dy'. \quad (3)$$

By accounting for the coupling of wing sections through the downwash generated on the entire wing as in (3), the flow is three dimensional. However, the absence of spanwise flow in the long-wavelength limit makes the flow at each wing section approximately two dimensional.

Writing Eqs. (1)–(3) in terms of θ and expanding $\alpha^e(\theta)$ and $\Gamma(\theta)$ as two Chebyshev series, the integral equation reduces to a matrix equation which can be solved numerically. We then use Γ to compute the lift L by summing the circulation at each cross section,

$$L = -\rho U_0 \int_{-s}^s \Gamma(y) dy. \quad (4)$$

This model of a smooth elliptic wing predicts that the lift increases continuously with angle of attack [8]. The top surface of the wing has an adverse pressure gradient $p_x = dp/dx > 0$ over a large part of the wing, since pressure is minimum near the leading edge where the flow velocity $u(x)$ is maximum, and then increases towards the trailing edge. As α increases, the magnitude of this adverse pressure gradient also increases, until at a critical angle of attack the boundary layer separates over a large part of the wing, and the wing stalls [7]. For angles of attack above this critical angle the lift on the wing is severely reduced. Experimentally, for a smooth flipper with $s = 3.6$ m and $t/c = 0.23$, the critical angle is approximately 12° [3]. At stall, the lift coefficient $C_L = L/(\frac{1}{2}\rho U_0^2)$ on a wing section drops to about 0.6 [4], and results mainly from the vertical component of form drag.

How are the aerodynamic characteristics of the wing changed when bumps are added? To investigate this we analyze our model with a spanwise oscillating chord, and solve the integral Eq. (1)–(3) both numerically and by a series perturbation. The latter allows us to clarify the relative roles of the physical parameters in the problem (e.g., bump amplitude, wavelength, thickness/chord, etc.). We define the chord as $c(\theta) = c_0 \sin\theta(1 + \eta S)$, where η is the amplitude of the bumps and $S = \frac{1}{c_0} \sum_{k=1}^{\infty} a_k \cos(k\theta)$ describes the perturbation of the wing from a smooth elliptical wing. Simultaneously expanding the effective angle of attack and circulation in orders of thickness/chord

ratio $T = \frac{4}{3\sqrt{3}} t_0/c_0$ and bump amplitude η ,

$$\begin{aligned} \alpha^e(\theta) &= \alpha_{0,0}^e + \eta \alpha_{1,0}^e + T \alpha_{0,1}^e + \eta T \alpha_{1,1}^e + \dots, \\ \Gamma(\theta) &= \Gamma_{0,0} + \eta \Gamma_{1,0} + T \Gamma_{0,1} + \eta T \Gamma_{1,1} + \dots, \end{aligned} \quad (5)$$

where each $\alpha_{i,j}^e$ is expressed as a Chebyshev series,

$$\alpha_{i,j}^e = \sum_{q=1}^{\infty} b_q^{i,j} \frac{\sin q\theta}{\sin\theta}, \quad (6)$$

and using (1) it can be shown that

$$\begin{aligned} \Gamma_{0,0} &= -\pi U_0 c_0 \alpha_{0,0}^e; \\ \Gamma_{1,0} &= -\pi U_0 c_0 (\alpha_{1,0}^e + S(\theta) \alpha_{0,0}^e); \\ \Gamma_{0,1} &= -\pi U_0 c_0 (\alpha_{0,1}^e + \alpha_{0,0}^e); \quad \text{etc.} \end{aligned} \quad (7)$$

These equations can be solved to any desired order of η and/or T . We mention the resulting coefficients $b_q^{i,j}$ here to first order (in subsequent calculations we go to second order, i.e., $O(\eta^2, T^2, \eta T)$),

$$\begin{aligned} b_1^{0,0} &= \frac{\alpha}{1 + \frac{\pi c_0}{4s}} \quad \text{all other } b_q^{0,0} = 0, \\ b_1^{0,1} &= -\frac{\pi c_0}{4s} \frac{b_1^{0,0}}{1 + \frac{\pi c_0}{4s}} \quad \text{all other } b_q^{0,1} = 0, \\ b_1^{1,0} &= 0, \quad b_{q>1}^{1,0} = -\frac{\pi q}{8s} b_1^{0,0} \frac{a_{(q-1)\geq 1} - a_{q+1}}{1 + q \frac{\pi c_0}{4s}}. \end{aligned}$$

This series perturbation reproduces the aforementioned result that lift is proportional to α for an elliptic wing for which only $b_1^{0,0}$ and $b_1^{0,1}$ are relevant. Also note how the role of wavelength λ is introduced through the coefficients $b_{q>1}^{1,0}$, since $\lambda = 4s/q$. We restrict the choice of bump amplitude and wavelength to keep the total planform area constant. Since (3) is valid for a high aspect ratio wing (ratio of span to mean chord), errors are minimal as long as $s \frac{dC_L}{dy} \ll 1$ [7]. In our notation, this criterion becomes

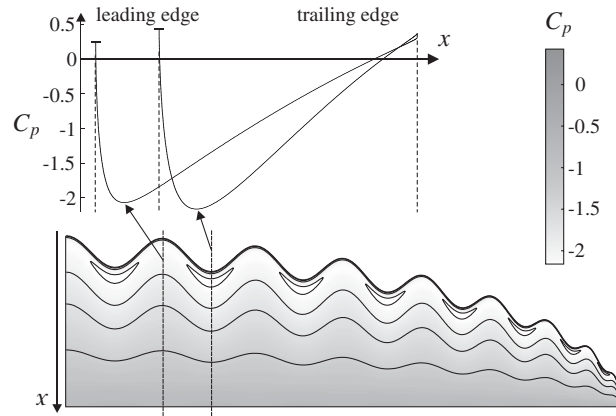


FIG. 2. (a) Calculated pressure profiles on top of a typical bump and trough and (b) calculated pressure distribution on the top of a bumpy wing. Note the pressure minimum in the troughs near the leading edge. Here, $\alpha = 6^\circ$, $\eta = 0.1$.

$4\pi \frac{\eta\alpha}{\sin\theta} \frac{s}{\lambda} \ll 1$. This model therefore operates in the small amplitude, small angle of attack, and long-wavelength limit; errors are introduced near the tip where $\sin\theta$ is small.

Figure 2 shows pressure contours for the top surface of a bumpy wing. Since neighboring bumps and troughs have similar thicknesses but different chords, the same pressure difference must be overcome over a shorter distance behind a trough than behind a bump. Hence the pressure gradient is more adverse behind troughs than behind bumps, and separation occurs first behind troughs.

Given the location of the separation point, we transpose the stall criterion from a smooth wing to a bumpy wing. We use a well known criterion for turbulent boundary layer separation to compute the location of the separation point x_s [10–12]. Using the nondimensional pressure coefficient $C_p = p(x)/(\frac{1}{2}\rho U_0^2)$, the criterion reads

$$F(x) = C_p \left(x \frac{dC_p}{dx} \right)^{1/2} \left(10^{-6} \text{Re} \right)^{-1/10}, \quad (8)$$

where if $\max[F(x)] \geq 0.40$, then $F(x_s) = 0.40$; if $0.35 \leq \max[F(x)] < 0.40$, then $F(x_s) = \max[F(x)]$ and finally if $\max[F(x)] < 0.35$, then separation does not occur. Note that the pressure coefficient C_p depends on x , as well as the Reynolds number which is defined as $\text{Re} = U_0 x / \nu$. This criterion was originally derived by matching an arbitrary imposed outer flow to the flow in the boundary layer, where the overall flow is assumed to be turbulent. Flow separation starts at the trailing edge and creeps forward with increasing angle of attack, in accordance with experiments. Any reasonable separation criterion will lead to the same qualitative flow features. The strength of this particular criterion is that it does not require detailed knowledge of the flow in the boundary layer.

We thus find $(x_s/c)_{\text{elliptic}}$ for a smooth wing at stall ($\alpha = 12^\circ$). To calculate when a bumpy wing is stalled, we assume that if at any cross section of the wing $x_s/c < (x_s/c)_{\text{elliptic}}$, this section is stalled. Sections stall independently of neighboring sections, which is reasonable in the long-wavelength limit since the flow is then predominantly chordwise and the cause of separation or stall will be the upstream flow rather than the flow in neighboring sections. Behind troughs the adverse pressure gradient is larger, and x_s is closer to the leading edge; therefore troughs stall at a lower angle of attack than the bumps.

In fact, the model shows that there is a strong relationship between the local thickness to chord ratio (t/c) and the local stall angle, as shown in Fig. 3(a). The bumps, with relatively small t/c , stall at higher angles of attack. Total lift on a partially stalled wing is computed by summing the lift at each cross section, where stalled sections contribute through the vertical component of the form drag as described before. The choice of post-stall lift characteristics is an empirical input into the model. Calculations show that the model is not very sensitive to these post-stall characteristics. Using a constant $C_L = 0.6$ as in Fig. 4(a) or a more

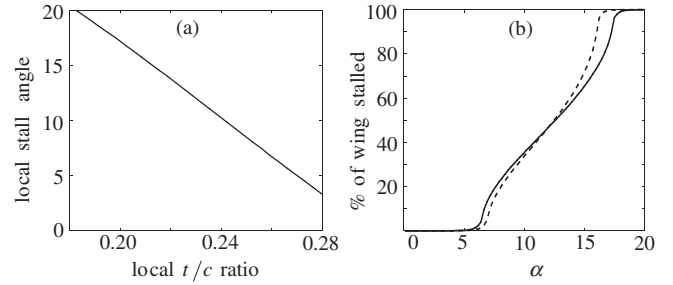


FIG. 3. (a) Local stall angle on a wing section calculated as a function of thickness to chord ratio, showing a monotonic decrease. (b) Percentage of wing area in stall for: (dashed line) uniform downwash terms, i.e., including $\alpha_{0,0}^e$ and $\alpha_{0,1}^e$ in (6) only and neglecting the influence of the bumps in the downwash; (solid line) full downwash including all $\alpha_{i,j}^e$ and thus the influence of the bumps ($\eta = 0.1$, $s = 3.6$ m, $k = 36$).

complex behavior resembling, e.g., the NACA 0018 post-stall lift curve [13] does not significantly alter the results.

We thus obtain the lift curve shown in Fig. 4(a), which may be compared with data from Johari *et al.* [4] as shown in Fig. 4(b). By design, the model shows a smooth wing stalling quite suddenly at $\alpha = 12^\circ$. For small amplitude perturbations (η) of this smooth wing, the transition to stall becomes slightly less abrupt, and for large η much of the wing near the troughs will be in stall at smaller angles of attack, so that the maximum lift coefficient of a smooth wing is never reached. Conversely, in order for the entire wing to be in stall even the most slender section near the bumps must stall. Hence the overall stall angle of the wing increases, in line with the experimental results. According to Fish & Battle [14], a typical humpback whale flipper has $\eta \approx 0.06$. For such amplitudes the lift curve flattens out at a fairly high C_L , and remains high until stall finally sets in at an angle of attack that is considerably larger than the stall angle of a smooth wing. Our model shows that the wavelength of the bumps has very little influence (Fig. 4); while wind tunnel data show a small dependence on wavelength.

There are two contributions to the flattening of the lift curve. First, by averaging a distribution of thickness/chord ratios along the wing, the lift curve is flattened out as the trough sections stall at lower angles of attack than the peak-sections, independent of the global flow coupling. A further flattening is caused by the global coupling between different wing sections that determine downwash as in (3). We may separate downwash into a spanwise uniform component which occurs for a smooth wing (i.e. including $\alpha_{0,0}^e$ and $\alpha_{0,1}^e$ in (6)) and an additional nonuniform component due to bumpiness (all other $\alpha_{i,j}^e$). In Fig. 3(b) we compare the proportion of wing area in stall with and without the nonuniform downwash component, and find that nonuniform downwash contributes to stall delay. The downwash is larger at the bumps relative to the troughs, leading to a decrease in effective angle of attack [see (2)], further delaying stall for the bumps. The variations in downwash

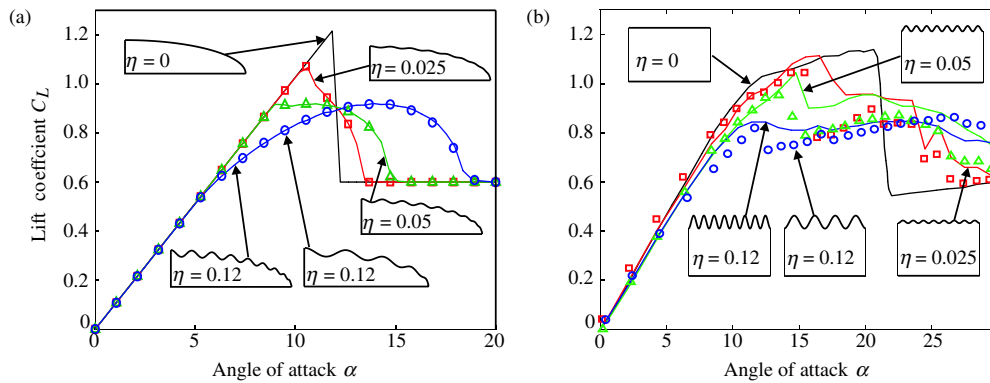


FIG. 4 (color online). Lift curves from (a) our model and (b) Johari *et al.* [4]. The black solid lines correspond to the unperturbed wing; the other solid lines correspond to 8 bumps per wing, while open symbols denote 4 bumps. Amplitudes are color coded: red $\eta = 0.025$; green $\eta = 0.05$; blue $\eta = 0.12$. In both (a) and (b), platform sketches are included for $\eta = 0, 0.025, 0.05$ and 0.12 .

along the wing are significant, especially when the wing is nearly in stall [see Fig. 3(b)].

In addition to predicting delayed stall, our calculations agree with many other aspects of the experiments. The observation that flow separation occurs first behind troughs is supported by wind tunnel experiments [4] and simulations [15]. The pressure contours in Fig. 2 predict that absolute pressure is lowest in troughs; water tunnel experiments show cavitation occurring there first [16]. Regarding drag, early simulations [17] and wind tunnel experiments suggested that bumpy wings might generate slightly more lift than smooth wings, and lower drag at angles of attack larger than the stall angle of a smooth wing. Our calculations do not show any appreciable difference in the induced drag generated by bumpy wings, but for short enough wavelengths, a very slight improvement in L/D_i can be observed, never much larger than 0.1% [18].

In conclusion, we note that our aerodynamic model captures the main features exhibited by wing section experiments, namely, a more gradual stall and a higher overall stall angle. The original experiments by Miklosovic *et al.* [3] showed a larger maximum lift coefficient and a somewhat sudden stall; neither our model nor the experimental work on wing sections reproduce these features. This discrepancy may be due to tip effects which cannot occur in the wing section experiments of Johari *et al.* [4], and cannot be described accurately by our current model as described before. Future work should address these tip effects, as well as the potential role of leading-edge vortices if these are found to be present.

It remains an open question why only humpback whales are observed to have these leading-edge bumps, and if indeed they are beneficial for the species. Gradual stalling and larger overall stall angles increase the range of α over which a wing or flipper contribute to maneuverability, while decreasing the unpredictability of lift forces near the stall transition. It is possible that the lessons learned from humpback whale flippers will soon find their way into the design of special purpose wings, hydrofoils, as well as wind turbine and helicopter blades.

We thank the Harvard MRSEC and the NSF Division of Mathematical Sciences for support of this research. We thank F. E. Fish for interesting references and discussions.

-
- [1] J. H. W. Hain, G. R. Carter, S. D. Kraus, C. A. Mayo, and H. E. Winn, *Fish. Bull.* **80**, 259 (1982).
 - [2] B. L. Woodward, J. P. Winn, and F. E. Fish, *J. Morphol.* **267**, 1284 (2006).
 - [3] D. S. Miklosovic, M. M. Murray, L. E. Howle, and F. E. Fish, *Phys. Fluids* **16**, L39 (2004).
 - [4] H. Johari, C. Henoch, D. Custodio, and A. Levshin, *AIAA J.* **45**, 2634 (2007).
 - [5] B. Stein and M. M. Murray, *Proceedings of Unmanned Untethered Submersible Technology, UUST05* (Autonomous Undersea Systems Inst., Lee, NH, 2005).
 - [6] C. Goudeseune, *Quiet Flyer* **11**, 18 (2006).
 - [7] B. Thwaites, *Incompressible Aerodynamics* (Dover, New York, 1960).
 - [8] G. K. Batchelor, *An Introduction to Fluid Dynamics* (Cambridge University Press, Cambridge, England, 1992).
 - [9] D. J. Acheson, *Elementary Fluid Dynamics* (Clarendon, Oxford, 1990).
 - [10] B. S. Stratford, *J. Fluid Mech.* **5**, 1 (1959).
 - [11] N. Curle and H. J. Davies, *Modern Fluid Dynamics, Incompressible Flow Vol. 1* (Van Nostrand, London, 1968).
 - [12] H. Takada, *J. Phys. Soc. Jpn.* **39**, 1106 (1975).
 - [13] H. J. Goett and W. K. Bullivant, *NASA Technical Report No. NACA-TR-647*, 1939.
 - [14] F. E. Fish and J. M. Battle, *J. Morphol.* **225**, 51 (1995).
 - [15] F. E. Fish and G. V. Lauder, *Annu. Rev. Fluid Mech.* **38**, 193 (2006).
 - [16] S. Lebental, Master's thesis, Duke University, 2006.
 - [17] P. Watts and F. E. Fish, *Proceedings the Intl. Symp. on Unmanned Untethered Submersible Technology, UUST01*, (Autonomous Undersea Systems Inst., Lee, NH, 2001).
 - [18] See EPAPS Document No. E-PRLTAO-100-073805 for some details of the calculations that went into our whale flipper model. For more information on EPAPS, see <http://www.aip.org/pubservs/epaps.html>.